Nonlinear Regression Based Health Monitoring of Hysteretic Structures Under Seismic Excitation

C. Xu[1,†], J. Geoffrey Chase[2] and Geoffrey W. Rodgers[2]

[1] *School of Astronautics, Northwestern Polytechnical University, Xi'an 710072, China*

[2] *Department of Mechanical Engineering, University of Canterbury, Private Bag 4800, Christchurch, New Zealand*

ABSTRACT

Structural health monitoring (SHM) provides a basis for rapid decision making under extreme conditions and can help ensure decisions are based on both accurate and timely information. Nonlinear hysteretic behaviour plays a crucial role in seismic performance-based analysis, design and assessment. This paper presents a health monitoring method using measured hysteretic responses. Acceleration and infrequently measured displacement are integrated using a multi-rate Kalman filtering method to generate restoring force-displacement hysteresis loops. A linear/nonlinear regression analysis based two-step method is proposed to identify nonlinear system parameters. First, hysteresis loops are divided into loading/unloading half cycles. Multiple linear regression analysis is applied to separate linear and nonlinear half cycles. Pre-yielding stiffness and viscous damping coefficient are obtained in this step and used as known parameters in the second step. Then, nonlinear regression analysis is applied to identified nonlinear half cycles to yield nonlinear system parameters and two damage indicators: cumulative plastic deformation and residual deformation. These values are closely related to structural status and repair costs. The feasibility of the method is demonstrated using a simulated shear-type structure with different levels of added measurement noise and a suite of ground motions. The results show that the proposed SHM method effectively and accurately identifies physical system parameters with up to 10% RMS

† Corresponding author. Tel.: +86 029 88493620
E-mail address: chao_xu@nwpu.edu.cn (C. Xu).

added noise. The resulting damage indicators can robustly and clearly indicate structural condition over different earthquake events.

KEY WORDS: structural health monitoring; nonlinear regression; hysteresis loops; damage identification; system identification

1. INTRODUCTION

Whenever a strong motion earthquake occurs, buildings are expected to remain standing with various degrees of damage. Critical decisions must be made within a short period of time concerning whether the buildings is suitable for continued occupancy. Vibration-based structural health monitoring (SHM) has gained much interest and attention in the civil engineering community in recent years. It is recognised as a powerful tool to identify damage at its earliest stage and to determine the residual useful life of structures, especially for rapid evaluation after a major event [1].

Many vibration-based SHM methods for civil structures are based on identifying changes in modal characterises [2-5]. However, only low frequency modes related to structural global deformation can be measured accurately, and these modal parameters are insensitive to localized damage in some cases and typically more applicable to structures where vibration response is highly linear [6]. Local diagnostic methods, such as impedance-based [7] and guided-wave based [8] methods, have been developed to improve sensitivity to local failure modes. However, they rely on close proximity to damage location and typically require many sensors distributed throughout a structure, which is currently impractical.

Advanced signal processing tools, such as wavelet analysis [9], empirical mode decomposition and Hilbert transform [10], are also being proposed. These techniques offer the advantage of determining both the location and time of the damage. However, they cannot directly identify physical system parameters and quantify the level of nonlinear damage due to the absence of a physical system model. Therefore, a number of model-based system identification methods have been presented, including a range of time-domain filters to track

time-variant model parameters [11-18]. However, only a few address nonlinear hysteresis and hysteresis-based damage indicators [19].

Hysteretic behaviour plays a critical role not only in seismic performance-based analysis and design [20-21], but also in capturing the nonlinear yielding and energy absorption associated with damage [23]. A SHM method that captures hysteretic response would give more insight into structural nonlinearity and quantify the level of nonlinear damage.

Structural restoring force-displacement hysteresis loops can be constructed from measured responses [24-26]. Accelerometers are the most commonly used instruments in civil structures, and displacement and velocity have to be obtained from numerical integration. This procedure is fraught with major pitfalls due to the effects of noise, limiting accuracy of the hysteretic loops and damage detection methods based on hysteresis monitoring. However, recent advances in low-rate displacement sensors, such as GPS [27], enable sensor fusion methods that deliver accurate displacement, velocity and acceleration. Several sensor fusion methods, such as the multi-rate Kalman filtering method [28], the cubic spline displacement correction method [29], the finite difference FIR filter method [30] and the finite element FIR filter method [31], have been proposed. These methods are expected to suppress measurement noise effectively and yield high quality hysteresis loops.

Structural damage indicators can be further extracted from constructed hysteresis loops. Secant stiffness was first calculated to determine the occurring of degradation and damage in [32]. System effective stiffness was extracted to describe the evolution of the structural stiffness in [33]. Evolution of hysteresis loop shape was considered as a rapid visual indicator of system degrading in [34]. Although these damage indicators can be used to indicate the

occurrence of damage, they are largely qualitative. Damage indicators that can quantify structural damage and closely related to structural post-event safety and repair costs are urgently needed.

This research presents a simple and novel health monitoring method for hysteretic structures subjected to seismic excitation. A multi-rate Kalman filtering technique is applied to estimate high quality displacement and velocity from high-rate sampled acceleration and low-rate sampled displacement data. Hysteresis loops are constructed and a regression analysis based two-step method is proposed to identify pre-yielding, viscous damping coefficient, yielding displacement and post-yielding stiffness, and resulting nonlinear damage indicators. The feasibility and robustness of the proposed method is illustrated for different noise levels over a suite of earthquake events.

2. CONSTRUCTION OF HYSTERESIS LOOPS

Toussi and Yao [24] first presented the idea of generating system hysteresis loops from recorded seismic response data. For this proof-of-concept study, it will be assumed that the structure in question can be adequately modelled as a single-degree-freedom (SDOF) system for simplicity and clarity. This situation is also true if the test structure responds primarily in a single mode, and can be defined:

$$m\ddot{x} + f(x, \dot{x}) = -m\ddot{x}_g \tag{1}$$

where x, $\dot{x}$ and $\ddot{x}$ are displacement, velocity and acceleration related to the ground; f is the total restoring force; $\ddot{x}_g$ is ground acceleration and m is the mass.

Rewriting Equation (1) and including viscous damping restoring force yields:

$$f(x, \dot{x}) = -m\left[\ddot{x}_g + \ddot{x}\right] = -mu = c\dot{x} + f_s(x, \dot{x}) \tag{2}$$

where u is absolute acceleration; c is viscous damping coefficient and $f_s(x, \dot{x})$ is stiffness restoring force. Assuming m to be known *a priori* and u to be measured, f is consequently obtained. Dynamic displacement and velocity can be obtained from measured sensor data by integration and correction. Thus, hysteresis loops can be constructed by graphing the restoring force versus displacement with time as an implicit parameter.

Direct integration of measured acceleration to obtain velocity and displacement is sensitive to noise and can cause significant distortion of estimated displacement [35]. Data fusion of high-rate acceleration and low-rate displacement measurements can effectively suppress noise and yield good estimates of velocity and displacement. If high-rate acceleration and

low-rate displacement measurements are available, estimation of displacement and velocity from the measurements can be modelled by a discrete dynamic system:

$$\boldsymbol{x}_{k+1} = \boldsymbol{A}^s \boldsymbol{x}_k + \boldsymbol{B}^s u_k + \boldsymbol{\alpha}_k \tag{3}$$

$$z_k = \boldsymbol{H}_k \boldsymbol{x}_k + \boldsymbol{\beta}_k \tag{4}$$

where Equation (3) is the system equation and Equation (4) is the observation equation, u_k is the measured acceleration and z_k is the measured displacement. The state vector $\boldsymbol{x}_k$ comprises the displacement d_k and the velocity v_k, i.e.,

$$\boldsymbol{x}_k = \begin{bmatrix} d_k \\ v_k \end{bmatrix} \tag{5}$$

Note that the sub-index *k* indicates a progression in time. $\boldsymbol{A}^s$ is a 2×2 matrix describing the system dynamics, $\boldsymbol{B}^s$ is 2×1 input matrix and $\boldsymbol{H}_k$ 1×2 design matrix, defined:

$$\boldsymbol{A}^s = \begin{bmatrix} 1 & \tau_a \\ 0 & 1 \end{bmatrix}; \quad \boldsymbol{B}^s = \begin{bmatrix} \tau_a^2/2 \\ \tau_a \end{bmatrix}; \quad \boldsymbol{H}_k = [1 \quad 0] \tag{6}$$

where τ_a is the acceleration sampling interval. In Equations (3) and (4), $\boldsymbol{\alpha}$ is a vector of acceleration measurement noise with distribution $(\boldsymbol{0}, \boldsymbol{Q}^s)$ and $\boldsymbol{\beta}$ is the vector of displacement measurement noise with distribution $(\boldsymbol{0}, \boldsymbol{R}^s)$. Both are assumed to be Gaussian white noise processes with covariance *q* an *r*. Thus, $\boldsymbol{Q}^s$ and $\boldsymbol{R}^s$ are given by**:**

$$\boldsymbol{Q}^s = \begin{bmatrix} q\,\tau_a^3/3 & q\,\tau_a^2/2 \\ q\,\tau_a^2/2 & q\tau_a \end{bmatrix}; \quad \boldsymbol{R}^s = \frac{r}{\tau_d} \tag{7}$$

where τ_d is the displacement sampling interval.

With Equations (3) to (7), a discrete time multi-rate Kalman filter can be used to estimate the displacement and velocity at each acceleration sampling instant [28,36].

3. SHM BASED ON REGRESSION ANALYSIS OF HYSTERESIS LOOPS

Many civil structures exhibit hysteresis when subject to severe cyclic loading. Figure 1 shows general hysteretic loops without considering system stiffness or strength degradation. A hysteretic cycle consists of a loading and an unloading half cycle. Any loading/unloading half cycle can be further divided into two nearly linear regimes: elastic and plastic, governed by k_e , the pre-yielding stiffness and k_p , the post-yielding stiffness, respectively. The elastic-plastic transition is generally smooth and gradual, but small. Omitting the transition process, the original half cycle can be represented by two line segments with different slopes, as shown in Figure 1, to capture the essential system dynamics.

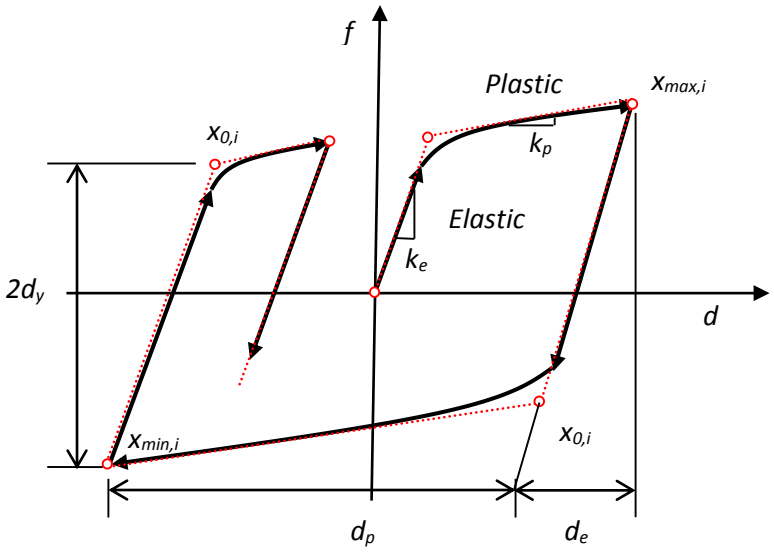

Figure 1 Hysteretic loops for arbitrary response

If the approximated two lines and their interaction point are found, the nonlinear plastic deformation during the half cycle can be easily calculated. Damage indicators related to post-event structural safety and repair costs, such as residual deformation and cumulative plastic deformation, can then be directly obtained by summing identified nonlinear deformation from all half cycles. Thus, the SHM problem is converted to a search for this approximation for each half cycle.

Hysteretic loops can be divided into many loading or unloading half cycles by identifying the points where the sign of the velocity changes. During a seismic event, structural behaviour is linear for most half cycles and nonlinear for fewer others. For linear half cycles, a single segment line approximation is enough. For nonlinear half cycles, a broken line approximation is needed. Hence, a two-step approximation method is developed to optimally approach the original half cycle. In the first step, linear and nonlinear half cycles are separated. In the second step, identified nonlinear half cycle are further estimated.

Regression analysis is a powerful tool for modelling the relationship between a dependent variable and one or more independent variables [37]. Recalling Equation (2), displacement x and velocity $\dot{x}$ are defined as the independent variables and restoring force f as the dependent variable. Thus, the optimal approximation of each half cycle formulates a regression problem.

3.1 Step 1: linear regression to each half cycle

Multiple linear regression is applied to each half cycle. It is equal to use an equivalent linear system assumption to each half cycle. Thus, Equation (2) can be rewritten:

$$-m[\ddot{x}_g + \ddot{x}] = c_l\dot{x} + k_l x \tag{8}$$

where k_l is the effective system stiffness and c_l is the effective system damping. All observation variables $(x, \dot{x}, \ddot{x}, \ddot{x}_g)$ can be obtained directly or indirectly from measurements. Structural mass is assumed known a priori. Equation (8) holds at each sampling instant *k*, with variables defined:

$$y_k = -m[\ddot{x}_{gk} + \ddot{x}_k] \tag{9a}$$

$$x_{1,k} = \dot{x}_k \tag{9b}$$

$$x_{2,k} = x_k \tag{9c}$$

The optimal approximation problem can be formulated as:

$$\boldsymbol{Y} = \boldsymbol{X}\boldsymbol{\beta} + \boldsymbol{\epsilon} \tag{10a}$$

$$\boldsymbol{Y} = \begin{Bmatrix} y_1 \\ y_2 \\ \vdots \\ y_k \\ \vdots \\ y_n \end{Bmatrix}, \quad \boldsymbol{X} = \begin{bmatrix} 1 & x_{1,1} & x_{2,1} \\ 1 & x_{1,2} & x_{2,2} \\ \vdots & \vdots & \vdots \\ 1 & x_{1,k} & x_{2,k} \\ \vdots & \vdots & \vdots \\ 1 & x_{1,n} & x_{2,n} \end{bmatrix}, \quad \boldsymbol{\beta} = \begin{Bmatrix} \beta_0 \\ \beta_1 \\ \beta_2 \end{Bmatrix}, \quad \boldsymbol{\epsilon} = \begin{Bmatrix} \epsilon_1 \\ \epsilon_2 \\ \vdots \\ \epsilon_k \\ \vdots \\ \epsilon_n \end{Bmatrix} \tag{10b}$$

where n is the number of all observed response variable pairs, $\boldsymbol{Y}$ is regressand, $\boldsymbol{X}$ is the repressor, $\boldsymbol{\beta}$ is the regression coefficients vector to be estimated, and $\boldsymbol{\epsilon}$ is the vector of estimation error due to measurement noise and model error and is random and normally distributed. The least squares method then finds the unbiased estimates of the regression coefficients:

$$(b_0, b_1, b_2) = \mathbf{arg}\,\boldsymbol{min}_{\boldsymbol{\beta}}[(\boldsymbol{Y} - \boldsymbol{X}\boldsymbol{\beta})'(\boldsymbol{Y} - \boldsymbol{X}\boldsymbol{\beta})] \tag{11}$$

where the vector (b_0, b_1, b_2) is the estimates of the regression coefficients of $(\beta_0, \beta_1, \beta_2)$.

Comparing Equations (10) and (8), it is clear that the least squares estimates, b_1 and b_2, are the effective linear system damping and the effective stiffness coefficient, respectively. When there is no plastic deformation presented in the half-cycle, k_l should approach the system true pre-yielding elastic stiffness, k_e, and when there is nonlinear plastic deformation, $k_l$should capture a secant average stiffness of k_e and k_p. Therefore, k_l is similar to the secant stiffness in [32], but derived in a least squares sense here.

The estimated equivalent stiffness k_l can vary over different half cycles. Varying k_l is a significant indicator of the nature of the dynamic system. It is reasonable that the hysteresis curve is linear when the half cycle displacement increment Δd is small and nonlinear when Δd is larger than the structural yield displacement. A rapid drop in k_l at large displacement increment can be viewed as a good indicator of occurring inelastic behaviour during that half cycle. Thus, the plot of k_l versus Δd will be used to identify the potential nonlinear half cycle.

In addition, the estimated equivalent linear damping coefficient c_l is the measure of system energy dissipation. System energy dissipation capacity will increase due to the added hysteretic damping. The plot of c_l versus Δd may also be used as another indicator of the inelastic half cycles. Thus, linear and nonlinear half cycles can be separated by using a threshold determined from these indicators.

For all identified linear half cycles, the multiple linear regression process yields many estimates of viscous damping coefficient c and pre-yielding elastic stiffness k_e. The statistical mean of c and k_e over all these linear half cycles will be considered as 'true' values and be used as known parameters for the next step.

3.2 Step 2: nonlinear regression analysis to identified nonlinear half cycles

The post-yielding stiffness is typically about a 5%-10% of pre-yielding stiffness for many civil structures. Thus, the slope of the hysteresis curve for a nonlinear half cycle will undergo sudden change. To optimally approximate the nonlinear half cycles, data points in these nonlinear half cycles must be divided into multiple segments, and regress a different linearly parameterized polynomial for each segment. k_e and k_p can be obtained directly from estimated regression coefficients. The difficulty is associated with the unknown interaction

point of each segment and the joint point of the segmented regression lines has to be estimated. It is actually a special nonlinear regression problem, named multi-phase linear regression.

This nonlinear regression problem has a long history in mathematics [38-40] and has been applied in some engineering fields [41]. However, it is has not been used extensively in civil engineering. Let$(x_{k,}y_k), k = 1, \dots, n,$ be n pairs of observation values of displacement and the restoring force within a nonlinear half cycle. Because the viscous damping coefficient c is estimated from the first identification step, the stiffness restoring force can be calculated:

$$f_s(x, \dot{x}) = -m[\ddot{x}_g + \ddot{x}] - \tilde{c}\dot{x} \tag{12}$$

where $\tilde{c}$ is the estimated viscous damping coefficient from the first step. To optimally approximate the nonlinear half cycles, a multi-phase linear regression model can be defined:

$$\begin{cases} f_1 = a_1 x + b_1, & x_1 \le x \le x_0 \\ f_2 = a_2 x + b_2, & x_0 < x \le x_n \end{cases} \tag{13}$$

where $\boldsymbol{\alpha} = \{a_1, b_1, a_2, b_2\}^T$ is the set of the unknown regression coefficients of each segment and $x_0$is the unknown interaction point. The interaction point satisfies the linear constraint to ensure the continuity of the solution at the interaction point:

$$a_1 x_0 + b_1 = a_2 x_0 + b_2 \tag{14}$$

Using a least squares method, it is possible to seek the best estimate of the vector $\boldsymbol{\alpha}$, which minimize the residual sum

$$R(\boldsymbol{\alpha}) = \sum_{x_1 \le x_k \le x_0} [y_k - (a_1 x_k + b_1)]^2 + \sum_{x_n \ge x_k > x_0} [y_k - (a_2 x_k + b_2)]^2 \tag{15}$$

and subject to the constraint Equation (14).

To minimize the function $R(\boldsymbol{\alpha})$, a method similar to the one implemented in [41] is used here. Conceptually, if the transition point is known, the minimum of $R(\boldsymbol{\alpha})$ can be found by

computing a standard linear regression for each segment. Thus, given a specific division between data points I and $I+1$, the residual sum can be minimized over $\tilde{\boldsymbol{\alpha}}_{\boldsymbol{I}} = \{a_1, b_1, a_2, b_2\}^T$, and this outcome yields a sequence of residual sum functions $R_I(\boldsymbol{\alpha})(I = 2, \dots, n-2,)$. The goal is to pick the I that gives the minimum value for $R_I(\boldsymbol{\alpha})$. Note that this is true only when $x_I \leq x_0 \leq x_{I+1}$. The estimator of x_0 has to be computed using the linear constraint Equation (14) from the elements of $\tilde{\boldsymbol{\alpha}}_{\boldsymbol{I}}$ to check that x_0 is in fact between the two data points I and $I+1$ to ensure the solution is the final solution. Using the proposed nonlinear regression analysis method, each nonlinear half cycle is approached by a two-segment broken line. This process yields the estimates of post-yielding stiffness and yielding turning point on each nonlinear half cycle.

3.3 Damage Indicators

Information obtained from the proposed two-step method can be used to derive important damage indicators related to damage severity and repair cost of the target structure. In particular:

1) The pre-yielding and post-yielding stiffness, k_e and k_p, give good approximation of the actual system mechanical behaviour. k_p clearly indicates the system residual load carrying capacity after yielding. The k_p to k_e ratio, like bilinear factor α, can be used as a damage indicator to represent the sacrificial or residual stiffness during seismic events. Finally, changes in k_p and k_e over time indicate system stiffness/strength degradation.
2) The yielding turning points identified in Step 2 are related to system yield deformation, d_y. It can be seen from Figure 1 that for an unloading half cycle *i*:

$$d_{yi} = \frac{x_{max,i} - x_{0,i}}{2} \tag{16}$$

where $x_{max,i}$ is the displacement history maximum during the half cycle, $x_{0,i}$ is estimated interaction point of the half cycle *i*. For a loading nonlinear half cycle *i*:

$$d_{yi} = \frac{x_{0,i} - x_{min,i}}{2} \tag{17}$$

where $x_{min,i}$ is the displacement history minimum during the half cycle i.

3) Cumulative plastic deformation can be used to capture the accumulation of damage sustained during dynamic loading. It can be calculate by summing the absolute plastic deformation over all nonlinear half-cycles. The nonlinear plastic deformation d_p for an unloading half cycle i can be calculated:

$$d_{pi} = \left(x_{min,i} - x_{0,i}\right) \times \left(1 - \frac{k_p}{k_e}\right) \tag{18}$$

and for a loading half cycle i :

$$d_{pi} = \left(x_{max,i} - x_{0,i}\right) \times \left(1 - \frac{k_p}{k_e}\right) \tag{19}$$

Thus, the cumulative plastic deformation d_{net} is defined:

$$d_{net} = \sum_{i=1}^{nl} \left| d_{pi} \right| \tag{20}$$

and the residual deformation d_{rel} is defined:

$$d_{rel} = \sum_{i=1}^{nl} d_{pi} \tag{21}$$

where nl is the number of identified half cycles.

Other damage indices may also be easily obtained based on identified parameters. The more important point is that with the estimated physical system parameters, model validation and response prediction for future seismic event is also possible, which will give a further critical reference for evaluation of structural safety and repair costs. Finally, quantified knowledge of these values could provide a better foundation for decision making by building owners, tenants and insures, reducing debate and speeding up recovery.

4. SIMULATED PROOF-OF-CONCEPT STRUCTURE

The simulated proof-of-concept structure is a SDOF moment-resisting frame model of a five-story building shown in Figure 2. The seismic weight per floor is 1692 kN for the roof level and 2067 kN for all other levels. The frame system is designed using the displacement-based design approach to sustain a target drift of 2% under a 500-year return period earthquake. A push-over analysis shows bilinear behaviour between base-shear and roof displacement with yield deformation $d_y = 46.5\text{mm}$, pre-yielding stiffness k =27300kN/m and bilinear factor $\alpha = 0.065$. The estimated linear structural fundamental period is ~1.20s. The detailed nonlinear push-over results can be found in [19]. A damping ratio of 5% is assumed which is common for civil structures and the corresponding viscous damping coefficient c is 521kN.s/m.

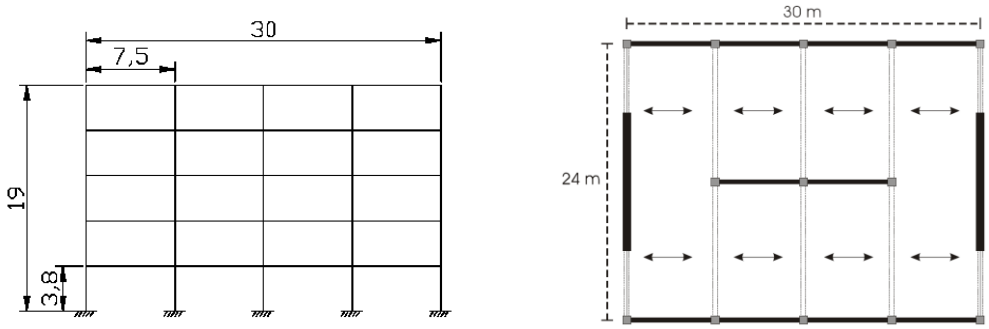

(a) front view (b) plan view

Figure 2 The simulated five-storey shear type building

Structural displacement and acceleration response is obtained through Newmark numerical integration. The sampling frequency is 200Hz for the measurement of acceleration and is 20Hz for the displacement. The objective of applying the proposed SHM method is to determine the structural properties of the pre-yielding stiffness, bi-linear factor, yielding deformation and estimate cumulative plastic deformation and residual deformation to indicate potential structural damage. The proposed method is implemented in MATLAB®.

First, the targeted structure was subjected to the 1987 Superstition Hill earthquake with peak ground acceleration (PGA) of 0.358g (EQ1 in Table 1). The SHM method was first demonstrated for proof of the concept using noise-free response signals. The effect of choices of the threshold to separate linear and nonlinear half cycles is investigated. Next, the effect of measurement noise was studied by adding a white noise process to acceleration and displacement response and ground acceleration, respectively. Four noise levels of 3%, 5% ,10% and 20% RMS noise-to-signal are considered. This case was repeated for 100 Monte Carlo runs to find the effect of noise and the range of possible variation at the given noise level.

Table 1 Selected 20 ground motions

EQ	Event	Year	M_w	Station	R-Distance(km)	Soil Type	Duration(s)	PGA(g)
EQ1	Superstition Hill	1987	6.7	EI Centro Imp. Co. Cent	13.9	D	40.0	0.358
EQ2				Brawley	18.2	D	22.0	0.156
EQ3				Plaster City	21.0	D	22.2	0.121
EQ4	Northridge	1994	6.7	Beverly Hills 14145 Muuhol	19.6	C	30.0	0.516
EQ5				Canoga Park – Topanga Can	15.8	D	25.0	0.356
EQ6				Glendale – Las Palmas	25.4	D	30.0	0.206
EQ7				LA – Hollywood Stor. FF	25.5	D	40.0	0.231
EQ8				N. Hollywood– Coldwater Can	14.6	C	21.9	0.273
EQ9				LA – N Faring Rd	23.9	D	30.0	0.298
EQ10				Sunland– Mt Gleason Ave	17.7	C	30.0	0.127
EQ11	Loma Prieta	1989	6.9	Capitola	14.5	D	40.0	0.529
EQ12				Gilroy Array #3	14.4	D	39.9	0.555
EQ13				Gilroy Array #4	16.1	D	40.0	0.417
EQ14				Gilroy Array #7	24.2	D	40.0	0.226
EQ15				Hollister Diff. Array	25.8	D	39.6	0.269
EQ16				Saratoga – W Valley Coll.	13.7	C	40.0	0.332
EQ17	Cape Mendocino	1992	7.1	Fortuna –Fortuna Blvd	23.6	C	44.0	0.116
EQ18				Rio Dell Overpass– FF	18.5	C	36.0	0.171
EQ19	Landers	1992	7.3	Desert Hot Springs	23.3	C	50.0	0.385
EQ20				Yermo Fire Station	24.9	D	44.0	0.245

To assess the robustness of the proposed method over different ground motions, the simulated structures were subjected to a suite of 20 ground motions with different spectral characteristics and PGA, as shown in Table 1. These earthquake records are widely used in earthquake engineering [19]. In each case, the noise level of 10% RMS is considered.

It is noted that in this study the 10% RMS Gaussian white noise was selected as a typical to relatively large level of sensor noise for measured ground acceleration, structural acceleration and displacement [28]. It is also large enough to encompass typical reported acceleration and displacement sensor accuracy [27, 29-31]. In fact, measurement of 10% RMS means 99% of errors are in +/- 30% which is a large level for any random sensor noise. Examination of different noise levels is used to prove the robustness and sensitivity of the method to different levels of noise.

5. RESULTS AND DISCUSSIONS

5.1. Validation of the proposed method using noise-free response

Simulated noise-free high-rate acceleration and low-rate displacement responses were first used as inputs to reconstruct high-rate displacement and velocity using the multi-rate Kalman filtering method. These reconstructed responses, together with ground and response acceleration, are input to SHM procedure.

Figure 3 plots the identified equivalent linear system stiffness k_l and equivalent viscous damping coefficient c_l for each half cycle versus half cycle displacement Δd, respectively. The points in Figure 3 can be divided into two regimes according to the trend of variation. When the half cycle displacement is small, k_l and c_l are nearly constant because the structure behaves linearly. Both drop rapidly as the amplitude of displacement exceeds a critical value. Therefore, Figure 3 can be used a qualitative indicator of system linear or nonlinear behaviour during an earthquake. If all points are around a horizontal line, the structure can be viewed linear or nearly linear. Otherwise, nonlinear deformation should be considered. Based on Figure 3, a threshold can be assigned to separate linear and nonlinear regimes. In this case, the threshold of 0.11m is used and the effect of the choices will be investigated in next section.

All points in linear regions directly give estimates of pre-yielding stiffness and viscous damping coefficient. Table 2 gives the statistical results of these two parameters. It can be seen that the identified mean of k_{e} is very close to the true model values with relative error of 0.1%. Since viscous damping restoring force forms a very small part of the total restoring

force, the mean estimate error of the viscous damping coefficient is a litter larger but still satisfying. Overall, the results demonstrate that the proposed method can give good estimates of system pre-yielding stiffness and viscous damping coefficient.

Table 2 Estimations of pre-yielding stiffness [KN/m] and viscous damping coefficient [KN.s/m]

	Mean	Mean error	St.d	95% confidence interval	True value
Pre-yielding stiffness	27335	0.1%	271	[27263, 27407]	27300
viscous damping coefficient	482	7.5%	108	[453, 510]	521

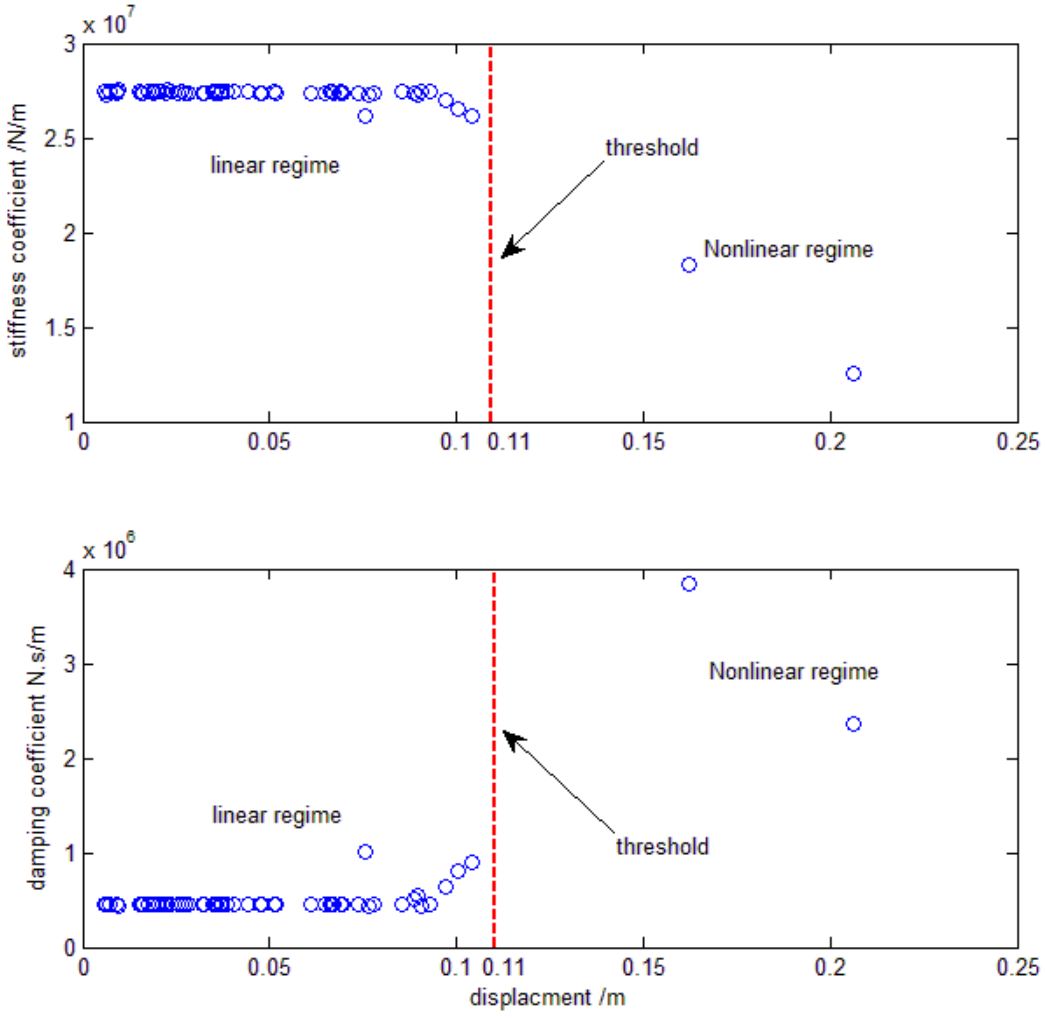

Figure 3 Linear regression results: (top) effective stiffness with half-cycle displacement; (bottom) effective viscous damping with half-cycle displacement

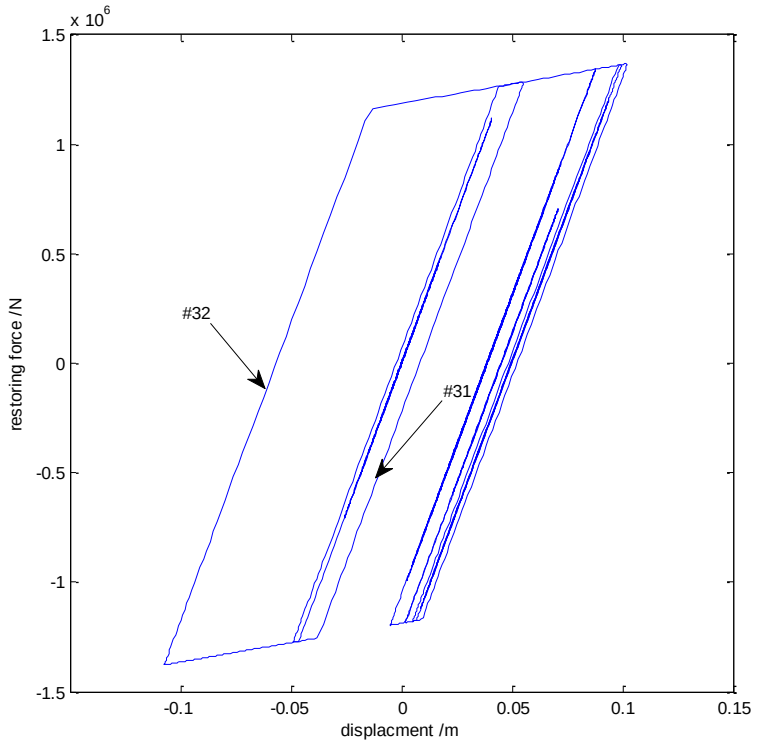

Figure 4 Simulated hysteresis loops

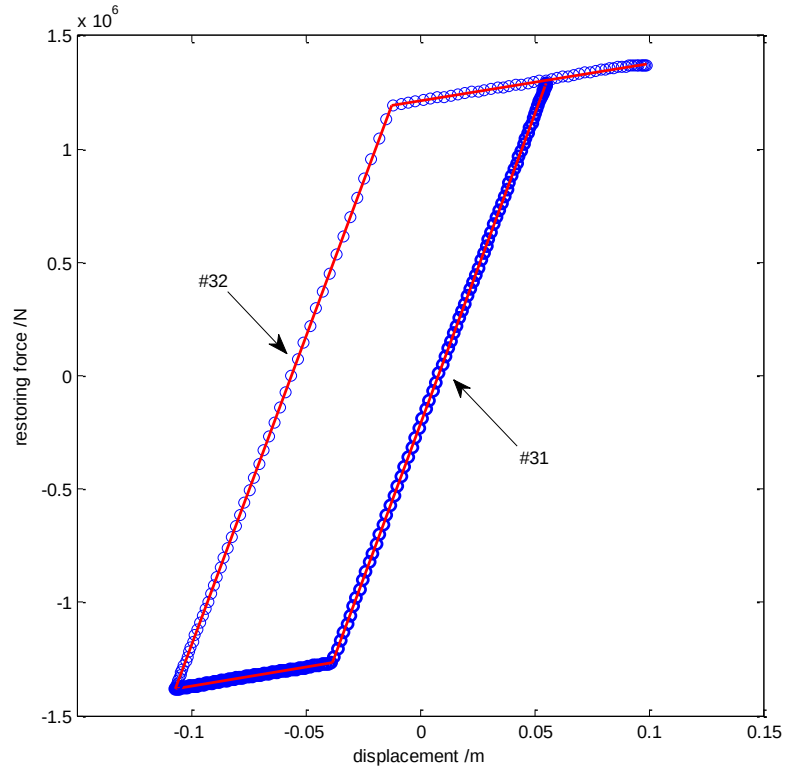

Figure 5 Identified nonlinear half cycles and multi-phase linear regression results for 2 half cycles. The line is the identified model and the circles are the simulated data.

Half cycles in nonlinear regime are identified using Step 2. Figure 4 shows the simulated true hysteresis loops. Figure 5 shows the identified nonlinear half cycles and multi-phase linear regression approximation results. It can be seen that using the threshold, the main nonlinear hysteretic half cycles are captured (#31, 32) that dominate the nonlinear structural behaviour. Multi-phase linear regression results approach the identified hysteresis half cycles very well. Table 3 shows the detailed multi-phase regression results for two half cycles, #31~32. It can be seen that the estimated bilinear factor and yield displacement are very close to the true parameters. The derived plastic displacement in each nonlinear half cycle can be summed to obtain the cumulative plastic deformation and residual displacement. In this case, the cumulative plastic deformation is 169.1mm and the residual displacement is +40.3mm.

Table 3 Estimated structural performance parameters from multi-phase linear regression analysis

Half Cycle #	Bi-linear factor	Yield displacement (mm)	Plastic displacement (mm)
31	0.062	46.7	-64.4
32	0.061	47.3	+104.7
Mean	0.062	47.0	/
Mean Error	4.6%	1.1%	/
True values	0.065	46.5	/

5.2. Effect of threshold chosen

The effect of the choice of threshold is investigated by varying its values between 0.09m and 0.13m. The results are listed in Table 4. It can be seen that there is little effect on the identification accuracy of the linear parameters, pre-yielding stiffness and viscous damping coefficient when the threshold chosen varies from 0.09m to 0.13m. However, identified bilinear factor and yield displacement shows a larger error when the threshold is lower because some linear or nearly linear half cycles are identified as nonlinear. In this situation, multi-phase linear regression will give poor results due to wrong regression model used. Thus, identification accuracy improves when only large displacement nonlinear half cycles are

considered (thresholds larger than 0.11m). However, it is noted that a very large threshold will mean some large displacement half cycles lost and underestimate the cumulative plastic deformation.

Table 4 Effect of threshold chosen on identification results

	Pre-yielding stiffness(KN/m)	Viscous damping (KN.s/m)	Yield deformation (mm)	Bilinear factor
True	27300	521	46.5	0.065
Threshold =0.09m				
Mean	27380	464	39.2	0.284
Coefficient of variation	0.007	0.174	0.356	1.581
Mean error	0.3%	10.9%	15.7%	336.9%
Threshold =0.10m				
Mean	27371	468	46.7	0.079
Coefficient of variation	0.007	0.176	0.010	0.702
Mean error	0.3%	10.2%	0.4%	21.5%
Threshold =0.11m				
Mean	27335	482	47.0	0.062
Coefficient of variation	0.010	0.224	0.008	0.008
Mean error	0.1%	7.5%	1.1%	4.6%
Threshold =0.12m				
Mean	27335	482	47.0	0.061
Coefficient of variation	0.010	0.224	0.008	0.008
Mean error	0.1%	7.5%	1.1%	6.2%
Threshold =0.13m				
Mean	27335	482	47.0	0.061
Coefficient of variation	0.010	0.224	0.008	0.008
Mean error	0.1%	7.5%	1.1%	6.2%

5.3 Effect of noise on parameter identification

Figure 6 shows the multi-phase linear regression analysis results for 100 runs at different noise levels. It can be seen that the as the noise level increases, the nonlinear regression accuracy and consistency both decrease. A threshold of 0.11m was used in all cases.

The statistical summary of identified system parameters compared to the true model parameters are listed in Table 5. It can be seen from Table 5 and Figure 6 that the numerical

accuracy of the identified parameters is generally very good and the two-step identification method proposed can give robust system performance parameters even at 10% RMS added noise level. In particular, the identified pre-yielding stiffness and yield displacement are less sensitive to noise than the viscous damping coefficient and bilinear factor. Even with added 20%RMS noise, the mean relative error of pre-yielding stiffness and yield displacement is within 2%. Thus, the identification of pre-yielding stiffness and yield deformation using the proposed method is highly robust to measurement noise. The identified bilinear factor is also excellent to 10% noise and good at 20%. It is more sensitive to noise due to there being far less data points in the nonlinear regime than in elastic regime, and regression analysis is sensitive to the number of data points. Identification accuracy would be improved if there were more large plastic displacements to provide a larger number of data points.

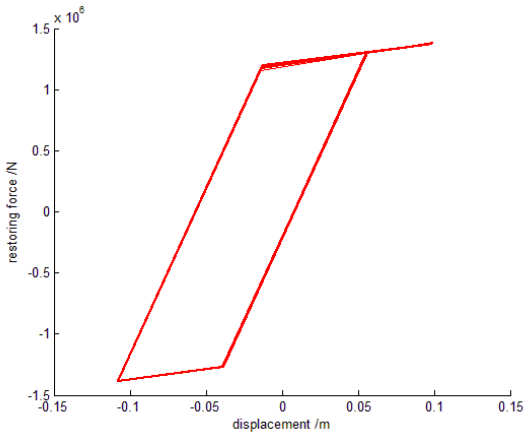

(a) 3% RMS noise

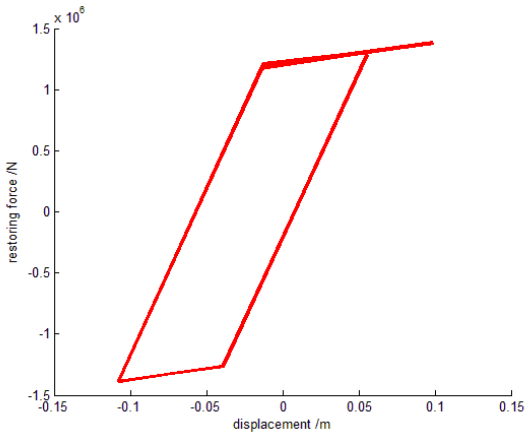

(b) 5% RMS noise

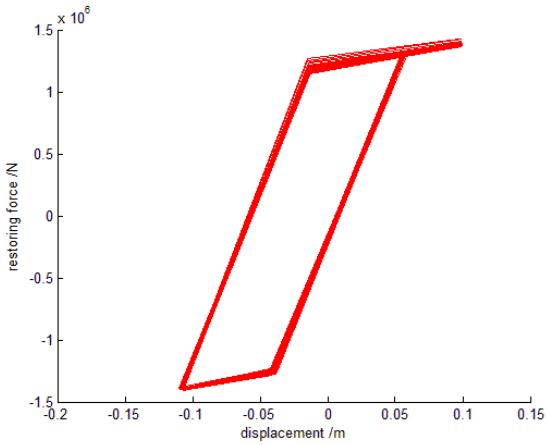

(c) 10% RMS noise

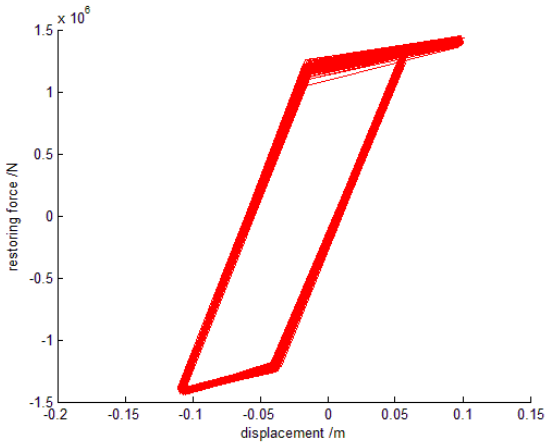

(d) 20% RMS noise

Figure 6 Identified nonlinear half cycles and multi-phase linear regression results

Table 5 Statistical summary of estimated system parameters for 100 Monte-Carlo runs (threshold =0.11m)

	Pre-yielding stiffness(KN/m)	Viscous damping (KN.s/m)	Bilinear factor	Yield deformation (mm)
Actual Model	27300	521	0.065	46.5
Noise-free				
Mean	27335	482	0.062	47.0
Coefficient of variation	0.0000	0.0000	0.0000	0.0000
Mean error	0.1%	7.5%	4.6%	1.1%
3%RMS white noise				
Mean	27335	481	0.062	47.1
Coefficient of variation	0.0000	0.0124	0.0212	0.002
Mean error	0.1%	7.7%	4.6%	1.3%
5%RMS white noise				
Mean	27336	482	0.064	47.2
Coefficient of variation	0.0018	0.0210	0.0345	0.0035
Mean error	0.1%	7.5%	1.5%	1.5%
10%RMS white noise				
Mean	27237	474	0.071	47.3
Coefficient of variation	0.0082	0.0625	0.0706	0.0080
Mean error	0.2%	9.0%	9.2%	1.7%
20%RMS white noise				
Mean	26825	440	0.092	46.9
Coefficient of variation	0.0142	0.1293	0.0855	0.0130
Mean error	1.7%	15.5%	41.5%	0.9%

5.4 Identification results over 20 seismic events

Tables 6 list the identified system parameters and damage indicators over 20 seismic events with 10%RMS added noise. A '-' is presented where the structure is identified as remaining linear during the event. The structure was identified as remaining linear for all of EQ2, 3, 5, 6, 9, 10,12,14, 17 and 19, and as nonlinear for the other events. Therefore, the proposed method can directly detect whether the structure undergoes nonlinear deformation. The identified system model parameters match very well with true model parameters and demonstrate the proposed method is robust to ground motions. The method can derive two damage indicators: cumulative plastic deformation and residual deformation, used to assess structural damage severity and repair costs. For example, estimated maximum cumulative plastic deformation is 500.4mm for EQ11, which indicates the structure is significantly damaged, while it is much lower for EQ7.

Table 6 Identification results for 20 seismic events with 10%RMS added noise

Event #	Pre-yielding stiffness (KN/m)	Yield displacement (mm)	bilinear factor	Viscous damping coefficient (KN.s/m)	Estimated cumulative plastic deformation (mm)	Residual deformation (mm)
EQ1	27237	47.3	0.071	474	168.1	42.0
EQ2	27421	-	-	448	-	-
EQ3	27218	-	-	500	-	-
EQ4	26870	51.0	0.108	544	391.5	54.7
EQ5	26971	-	-	557	-	-
EQ6	28119	-	-	480	-	-
EQ7	27411	45.8	0.141	475	21.1	20.0
EQ8	26967	46.0	0.200	577	214.7	33.4
EQ9	27622	-	-	461	-	-
EQ10	27531	-	-	453	-	-
EQ11	26723	46.7	0.154	512	500.4	9.3
EQ12	27571	-	-	453	-	-
EQ13	27346	44.6	0.131	468	198.1	30.0
EQ14	27819	-	-	478	-	-
EQ15	26976	47.1	0.112	506	98.3	60.8
EQ16	27016	47.4	0.123	521	368.0	91.9
EQ17	27470	-	-	463	-	-
EQ18	27289	46.6	0.126	480	234.6	64.0
EQ19	27540	-	-	459	-	-
EQ20	26974	46.9	0.128	503	307.7	97.9
True	27300	46.5	0.065	521		

It should be noted that there is no specific, direct comparative assessment of the proposed method against any existing SHM techniques. The primary reason is that to the best of the authors knowledge at this time, no prior, automated SHM methods split the linear half-cycles from the nonlinear half-cycles of response and pull out nonlinear half-cycle displacement and post-yielding stiffness. A possible exception is the work of Nayerloo et al [19], which is a much more complex, model-dependent algorithm. Equally importantly, the method of [19] is restricted to fitting a Bouc-Wen model, which is highly restrictive and can lose accuracy when the measured response is not similar to the underlying model employed. In contrast, the approach presented here is more general to any nonlinear, elasto-plastic method. Finally, it is important to note that we found no prior works that directly identified nonlinear stiffness in this fashion making direct comparison very difficult for those that do address nonlinear behaviour.

Although the efficiency of the method is demonstrated using a simple closed-formed problem, the value of the proposed method can be evaluated from three perspectives. First, the key of the method is to capture half-cycles and get elasto-plastic properties from them. Therefore, it is not dependent on any specific mechanics model, and relies only on direct measurements and identified half-cycles. Hence, the proposed method can be generalized to identify any form of hysteretic system with nonlinear half cycles, and the validation presented is not circularly dependent on the model while also being robust to the added noise.

Second, the identification procedure is carried out from half-cycle to half cycle. It thus can capture time-variant physical parameters to characterize a degrading hysteretic system. Finally, the identification procedure is essentially performed storey by storey. Therefore, the

proposed method is completely generalizable to overall nonlinear multi-storey structures and a wide range of mechanics.

However, the robustness of the method to real data is still partly unproven since the significant plastic real data is limited available. The proposed identification procedure remains to be experimentally validated and further test before implementation in the field for final performance evaluation.

Equally, it is critical to note that the model used in simulation does not affect this method which is effectively model-free, relying only on measurable, with noise, responses. The validation thus knows the results exactly to assess accuracy and equally is not tied to the model used to simulate the data, ensuring a robust validation

6. CONCLUSIONS

This paper develops a novel SHM method for civil structures using hysteresis loops reconstructed from seismic response data. Low-rate sampled displacement and high-rate sample acceleration are fused by the multi-rate Kalman filtering method to construct high quality hysteresis loops. A two-step regression analysis based method is developed to identify nonlinear system parameters and extract damage indicators related to structural health status and repair costs.

To apply linear and nonlinear regression analysis, system hysteretic loops are split into many half cycles where restoring force is a monotone function of displacement. A special nonlinear regression method, named multi-phase linear regression is used to directly estimate turning points and post-yielding stiffness. This approach significantly simplifies the nonlinear system identification procedure for obtaining pre-yielding stiffness, viscous damping coefficient, post-yielding stiffness and the yield displacement simultaneously.

From the results obtained in this study, it is clear that the proposed method is feasible and effective for nonlinear system identification and damage indicator extraction. When no measurement noise is added, the proposed SHM procedure can identify system physical parameters with very high precision. Even with 10% or 20% RMS noise, the method identifies some system parameters with good precision, and has good repeatability and robustness. The proposed method is also robust over different ground motions, and can directly detect whether nonlinear response occurs.

Overall, the proposed SHM method is simple, direct and robust. The identification procedure is performed time segment by time segment, which provides the possibility for it to be implemented in real-time or near real-time. Although the concept is proven focusing on structural systems that display non-degraded hysteresis behaviour, it can be easily extended to degrading structures and arbitrary changes in system parameters, including degradation.

ACKNOWLEDGMENT

The present work was supported in part by China Scholarship Council for post-doctoral fellow (No.201203070008) and National Science Foundation of China (No.11372246). The authors would like to thank the reviewers for their comments that help improve the manuscript.

REFERENCES

1. Naeim F. Real-Time Damage Detection and Performance Evaluation for Buildings [M]. Earthquakes and Health Monitoring of Civil Structures. Springer Netherlands, 2013: 167-196
2. Hearn G, Testa R B. Modal analysis for damage detection in structures [J]. Journal of Structural Engineering, 1991, 117(10): 3042-3063.
3. Doebling S W, Farrar C R, Prime M B. A summary review of vibration-based damage identification methods [J]. Shock and vibration digest, 1998, 30(2): 91-105.
4. Peeters B, Maeck J, De Roeck G. Vibration-based damage detection in civil engineering: excitation sources and temperature effects [J]. Smart materials and Structures, 2001, 10(3): 518.
5. Ko J M, Ni Y Q. Technology developments in structural health monitoring of large-scale bridges [J]. Engineering structures, 2005, 27(12): 1715-1725.
6. Chang PC, Flatau A, Liu SC. Review paper: Health monitoring of civil infrastructure. Structural health monitoring, 2003; 2(2): 257-267.
7. Park G, Cudney HH, Inman DJ. Impedance-based health monitoring of civil structural components. Journal of Infrastructure Systems (ASCE), 2000; 6: 153-160.
8. Raghavan A, Cesnik CES. Review of guided-wave structural health monitoring. *The Shock and Vibration Digest*, 2007; **39**(2):91-114.
9. Hou Z, Noori M, Amand RS. Wavelet-based approach for structural damage detection. *Journal of Engineering Mechanics* 2000; **126**(7):693-703.
10. Yang J N, Lei Y, Lin S, et al. Hilbert-Huang based approach for structural damage detection[J]. Journal of engineering mechanics, 2003, 130(1): 85-95.
11. Lin JS, Zhang YG. Nonlinear structural identification using extended Kalman filter [J]. Computers and Structures 1994; 52(4): 757-764.
12. Sato T, Qi K. Adaptive H∞ filter: its application to structural identification [J]. Journal of Engineering Mechanics (ASCE) 1998; 124:1233-1240.

13. Lob CH, Lin CY, Huang C-C. Time domain identification of frames under earthquake loading [J]. Journal of Engineering Mechanics (ASCE) 2000; 126:639-703.
14. Chase JG, Hwang KL, Barroso LR, Mander JB. A simple LMS-based approach to the structural health monitoring benchmark problem [J]. *Earthquake Engineering and Structural Dynamics* 2005; **34**:575-594.
15. Chase JG, Spieth HA, Blome CF, Mander JB. LMS-based structural health monitoring of a non-linear rocking structure. *Earthquake Engineering and Structural Dynamics* 2005; **34**:909-930.
16. Yang JN, Lin SL, Huang HW, Zhou L. An adaptive extended Kalman filter for structural damage identification [J]. *Structural Control and Health Monitoring* 2006; **13**:849-867.
17. Wu M, Smyth A W. Application of the unscented Kalman filter for real-time nonlinear structural system identification [J]. *Structural Control and Health Monitoring*, 2007, 14(7): 971-990.
18. Chen Y, Feng M Q. Structural health monitoring by recursive bayesian filtering [J]. *Journal of engineering mechanics*, 2009, 135(4): 231-242.
19. Nayyerloo M, Chase JG, MacRae GA, Chen XQ. LMS-based approach to structural health monitoring of nonlinear hysteretic structures [J]. *Structural Health Monitoring* 2011; **10**(4):429-444.
20. Christopoulos C, Pampanin S, Priestley MJN. Performance-based seismic response of frame structures including residual deformations, part I: single-degree of freedom systems. *Journal of Earthquake Engineering* 2003; **7**(1):97-118.
21. Pampanin S, Christopoulos C, Priestley MJN. Performance-based seismic response of frame structures including residual deformations, part II: multiple-degree of freedom systems. *Journal of Earthquake Engineering* 2003; **7**(1):119-147.
22. Iemura H, Jennings PC. Hysteretic response of a nine story reinforced concrete building. *Earthquake Engineering and Structural Dynamics* 1974; **3**:183-201.
23. Stephens JE, Yao TP. Damage assessment using response measurements. *Journal of Structural Engineering* (ASCE) 1987; **113:787**-801
24. Toussi S, Yao JTP. Hysteresis identification of existing structures. *Journal of Engineering Mechanics* (ASME) 1983; **109**:1189-1202.
25. Iwan WD, Cifuentes AO. A model for system identification of degrading structures. *Earthquake Engineering and Structural Dynamics* 1986; **14**:877-890.
26. Subia SR, Wang ML. Nonlinear hysteresis curve derived by direct numerical investigation of acceleration data. *Soil Dynamics and Earthquake Engineering* 1995; **14**:321-330.

27. Chan WS, Xu YL, Ding XL, Xiong YL, Dai WJ. Assessment of dynamic measurement accuracy of GPS in three directions. *Journal of Surveying Engineering* (ASCE) 2006; **132**(3):108-117
28. Smyth A, Wu ML. Multi-rate Kalman filtering for the data fusion of displacement and acceleration response measurements in dynamic system monitoring. *Mechanical Systems and Signal Processing* 2007; **21**:706-723.
29. Hann CE, Singh-Levett I, Deam BL, Mander JB, Chase JG. Real-time system identification of a nonlinear four-story steel frame structure-application to structural health monitoring. *IEEE Sensors Journal* 2009;**9**:1339-1346.
30. Lee H S, Hong Y H, Park H W. Design of an FIR filter for the displacement reconstruction using measured acceleration in low-frequency dominant structures [J]. International Journal for Numerical Methods in Engineering, 2010, 82(4): 403-434.
31. Hong Y H, Lee S G, Lee H S. Design of the FEM-FIR filter for displacement reconstruction using accelerations and displacements measured at different sampling rates[J]. Mechanical Systems and Signal Processing, 2013.
32. Cifuentes AO, Iwan WD. Nonlinear system identification based on modelling of restoring force behaviour. Soil Dynamics and Earthquake Engineering 1989; 8:2-8.
33. Benedetti D, Limongelli M P. A model to estimate the virgin and ultimate effective stiffnesses from the response of a damaged structure to a single earthquake [J]. Earthquake engineering & structural dynamics, 1996, 25(10): 1095-1108.
34. Iwan WD. R-SHAPE: a real-time structural health and performance evaluation system. Proceedings of the US-Europe Workshop on Sensors and Smart Structures Technology, 2002; 33–38.
35. Worden K. Data processing and experiment design for the restoring force surface method, part I: integration and differentiation of measured time data [J]. Mechanical Systems and Signal Processing, 1990, 4(4): 295-319.
36. Lewis F L, Xie L, Popa D. Optimal and robust estimation: with an introduction to stochastic control theory[M]. CRC, 2008.
37. Seber G A F, Lee A J. Linear regression analysis [M]. John Wiley & Sons, 2012.
38. Hodon JD. Fitting segmented surveys whose join points have to be estimated. Journal of the American Statistical Association 1966; 61:1097-1129.
39. Lerman PM. Fitting segmented regression models by grid search. Journal of the Royal Statistical Society. Series C (Applied Statistics) 1980;**29**(1):77-84.

40. Cologne J, Sposto R. Smooth piecewise liner regression splines with hyperbolic covariates. Journal of Applied Statistics 1994;**21**(4):221-233.
41. Stoimenova E, Datcheva M, Schanz T. Application of two-phase regression to geotechnical data. Pliska Stud. Math. Bulgar 2004; 16: 245-257.